Ships and Offshore Structures

ISSN: 1744-5302 (Print) 1754-212X (Online) Journal homepage: www.tandfonline.com/journals/tsos20

Effective notch stress, random fatigue limit, and non-linear damage accumulation-based CA-VA fatigue resistance similarity of welded joints in steel structures

Ruben Leonard Geert Slange, Marije Deul, Agnes Marie Horn & Henk Den Besten

To cite this article: Ruben Leonard Geert Slange, Marije Deul, Agnes Marie Horn & Henk Den Besten (31 May 2026): Effective notch stress, random fatigue limit, and non-linear damage accumulation-based CA-VA fatigue resistance similarity of welded joints in steel structures, Ships and Offshore Structures, DOI: 10.1080/17445302.2026.2675358

To link to this article: https://doi.org/10.1080/17445302.2026.2675358

SHIPS AND OFFSHORE STRUCTURES
https://doi.org/10.1080/17445302.2026.2675358

Effective notch stress, random fatigue limit, and non-linear damage accumulation-based CA-VA fatigue resistance similarity of welded joints in steel structures

Ruben Leonard Geert Slange [a], Marije Deul [b], Agnes Marie Horn[c] and Henk Den Besten [a]

[a]Maritime and Transport Technology, Delft University of Technology, Delft, The Netherlands; [b]TNO, Delft, The Netherlands; [c]DNV, Høvik, Norway

ABSTRACT

Fatigue is often a governing limit state for steel (maritime) structures operating in variable amplitude loading conditions. Arc-welded joints connecting the structural members are typically the weakest links, and accurate lifetime estimates are essential for structural design. However, a resistance formulation and damage accumulation model incorporating the mid- and high-cycle fatigue strength and mechanism contributions is not available. In particular, one containing explicitly defined damage reliability and confidence levels. A generalized random fatigue limit resistance formulation and a generalized non-linear damage accumulation model, including the variable amplitude loading induced fatigue limit degradation, are proposed to improve the lifetime estimates applicable for fatigue assessment in the frequency domain. The most likely fatigue resistance parameters are obtained by analysing fatigue resistance data from literature containing a broad range of loading distributions. Adopting the average effective notch stress as a fatigue strength parameter, including global mean stress effects, constant and variable amplitude fatigue resistance similarity is obtained, as reflected in a mean damage estimate of one. The fatigue lifetime estimate accuracy significantly improved in comparison to state-of-the-art guidelines and codes (e.g. IIW, DNV, BS). Consistent reliability and confidence levels for constant and variable amplitude fatigue assessment for design suggest an allowable damage of 0.2. A similar value for guidelines and codes illustrates over-conservatism from a fatigue resistance perspective.

ARTICLE HISTORY
Received 10 November 2025
Accepted 15 April 2026

KEYWORDS
Arc-welded joints; variable amplitude fatigue; effective notch stress; random fatigue limit; non-linear damage accumulation; reliability and confidence

Nomenclature

C	fatigue resistance curve intercept
$D(\mu, \sigma)$	random accumulated fatigue damage
D_μ	accumulated fatigue damage mean value
D_σ	accumulated fatigue damage standard deviation
$F(\cdot)$	cumulative distribution function
F_N	normal force
M_b	bending moment
N	fatigue lifetime in number of cycles
R	response ratio (S_{min}/S_{max})
S	fatigue strength parameter
$S_\infty(\mu, \sigma)$	random fatigue strength limit
$S_\infty(\mu, \sigma; D)$	damage-dependent random fatigue strength limit
S_e	effective notch stress range
S_h	hot-spot structural stress range
S_{max}	maximum S value
S^g_{mean}	global mean stress
S_n	nominal stress range
c_l	confidence level
$f(\cdot)$	probability density function
l_w	weld leg length
h_w	weld leg height
m	fatigue resistance curve slope
p_s	probability of survival
r	through-thickness coordinate
t_b	base plate thickness
t_c	cross/connecting/cover plate thickness
t_p	plate thickness, either t_b or t_c
$_i$	specimen index (N_i, S_i)
$_j$	VA response spectrum index (N_j, S_j, n_j)
$_h$	damage accumulation index (D_h)
γ	response ratio exponent
γ_E	Euler constant
ζ	fatigue limit degradation exponent
ρ	notch radius
ρ^*	material characteristic length
$\rho_{S\infty}$	mid- to high-cycle fatigue transition coefficient
σ_N	CA fatigue lifetime standard deviation
$\sigma_{N,VA}$	VA fatigue lifetime standard deviation
$\sigma_n(r/t_p)$	weld notch stress distribution
σ_{VA}	VA fatigue standard deviation
AIC	Akaike Information Criterion
CA	constant amplitude
GRFL	generalized random fatigue limit
GRNDA	generalized random non-linear damage accumulation
HCF	high-cycle fatigue
LCB	lower confidence bound

CONTACT Ruben Leonard Geert Slange r.l.g.slange@tudelft.nl Delft University of Technology, Mekelweg 2, 2628 CD Delft, Netherlands

LDA	linear damage accumulation
MCF	mid-cycle fatigue
MLE	maximum likelihood estimate
RLDA	random linear damage accumulation
UCB	upper confidence bound
VA	variable amplitude

1. Introduction

The response of maritime structures to variable wind and wave loading is cyclic and predominantly of the mode-I type (e.g. Bufalari et al. 2024). Fatigue: a local, progressive damage process consisting of initiation and growth contributions (Schijve 2009) is a governing limit state. For commonly applied metals like steel, arc-welded joints typically connecting the structural members are identified as the weakest links in that respect since the notched geometries introduce fatigue-sensitive stress concentrations; i.e. hot spots.

The constant amplitude (CA) fatigue resistance $N(S)$ relates the number of cycles N until a critical crack size or even fracture and a particular fatigue strength parameter S. In the crack growth controlled mid-cycle fatigue (MCF) region with N in the order of $10^4 \sim 5{\cdot}10^6$ cycles, typically a log–log linear dependency is observed, and the semi-empirical Basquin relation (e.g. Qin et al. 2021): $\log(N) = \log(C) - m{\cdot}\log(S)$; a Wöhler curve, is naturally adopted. Intercept $\log(C)$ and slope m are the strength and mechanism coefficients, respectively.

Shifting toward the high-cycle fatigue (HCF) region with N in the order of $5 \cdot 10^6 \sim 10^9$ cycles, the slope m typically increases, implying a change in fatigue damage mechanism, i.e. from crack growth to crack initiation dominated. The slope may tend to become even infinitely large, reflecting a fatigue limit: a threshold. Rather than being constant, the fatigue limit is observed to be a stochastic variable $S_\infty(\mu,\sigma)$, naturally introducing a random fatigue limit model (Leonetti et al. 2017): $\log(N) = \log(C) - m{\cdot}\log(S) - \rho_{S\infty}{\cdot}\log\{1 - S_\infty(\mu, \sigma)/S\}$ with $\rho_{S\infty}$ being the mid- to high-cycle fatigue transition coefficient. Since the far-field response of welded joints in steel maritime structures is predominantly linear elastic, S is typically of the stress – rather than strain or energy – type in particular, for MCF and HCF (Qin et al. 2021). Different fatigue strength parameters have been developed over time, balancing lifetime estimate accuracy, fatigue strength parameter complexity, and computational efforts (e.g. den Besten 2018; Qin et al. 2019). Incorporating local notch information provides more generalized S formulations, and the number of fatigue resistance curves for arc-welded joints reduces accordingly (i.e. ultimately to one), like for the effective notch stress $S = S_e$ (Bufalari et al. 2024), providing a generalized random fatigue limit formulation (Qin et al. 2021).

For variable amplitude (VA) fatigue, S may be different from one cycle to another. Using the maximum value S_{max}, the CA equivalent log–log linear Basquin relation can be established for the MCF region: $\log(N) = \log(C') - m'{\cdot}\log(S_{max})$; a Gassner curve (Sonsino et al. 2004; Sonsino 2007). However, S_{max} does not incorporate the VA structural response characteristics like the spectral properties or cycle history in respectively a frequency or time domain approach (Naess and Moan 2012), meaning that intercept $\log(C')$ and slope m' are case dependent and a generalized formulation is lacking.

Adopting a linear damage accumulation (LDA) model (Miner 1945), the mechanism as reflected in the slope is assumed to be the same for CA and VA conditions (i.e. $m' = m$): $D = \Sigma\{n_j(S_j)/N_j(S_j)\} = (N/C){\cdot}\Sigma\{(n_j(S_j)/N){\cdot}S_j^m\} \leq 1$. Introducing an equivalent stress S_{eq}, the Basquin relation becomes $\log(N) = \log(C') - m{\cdot}\log(S_{eq})$ with $S_{eq} = \Sigma\{(n_j(S_j)/N){\cdot}S_j^m\}^{1/m}$ incorporating each stress range S_j and corresponding number of cycles $n_j(S_j)$, i.e. the spectral properties without response history effects. Since intercept $\log(C') = \log(D{\cdot}C)$, the Gassner curves are basically a shifted Wöhler curve (e.g. Johannesson et al. 2005; Ciavarella et al. 2017). Since fatigue failure for several types of spectrum shape and content appears at $D \neq 1$, both conservative and non-conservative (e.g. Agerskov 2000; Gurney 2006; Fricke and Paetzold 2014), the allowed damage for fatigue design is typically a relatively small number $0 < D << 1$ (e.g. Sonsino 2010; Hobbacher and Baumgartner 2024), but seems often based on a qualitative assessment rather than a quantitative one involving damage reliability requirements and confidence bounds.

The VA structural response typically includes MCF and HCF contributions, cycles with larger and smaller S values, respectively, introducing a response history-dependent CA fatigue limit degradation for accumulating damage (Kunz and Kulak 1995); i.e. a response and resistance-induced damage accumulation non-linearity. Different damage models have been proposed (Bufalari et al. 2024). Incorporating the response part only (e.g. Fatemi and Yangt 1998; Hectors and De Waele 2021), typically $D = \Sigma[C_j{\cdot}\{n_j(S_j)/N_j(S_j)\}^{f(j)}] \leq 1$, considering the linear one as a special case for $C_j = f(S_j) = 1$. Simplifications typically concern a bi-linearization. A similar simplification can be adopted for the resistance part using dedicated Basquin formulations for the MCF and HCF region, reflected in the slope change (e.g. Hobbacher and Baumgartner 2024). Still, the LDA model $D = \Sigma\{n_j(S_j)/N_j(S_j)\} \leq 1$ can be employed. Considering the actual resistance characteristics, the fatigue limit decreases

with increasing D and becomes damage-dependent, i.e. $S_\infty(\mu, \sigma; D)$, meaning the damage accumulation calculation becomes an iterative process.

Introducing a damage exponent ζ, the response induced non-linearity – either convex or concave downward – is accounted for as well (e.g. Leonetti et al. 2020). To include the damage variability, a stochastic one is adopted: $D(\mu, \sigma) \leq 1$. However, the involved fatigue strength parameter is the nominal stress range S_n and does not allow for a generalized formulation nor a sufficiently large number of data sets to estimate the VA model parameters with high confidence.

Aiming for CA-VA fatigue resistance similarity in the MCF and HCF regions to obtain accurate VA fatigue lifetime estimates, S_e will be used as a fatigue strength parameter. The CA fatigue resistance formulation of arc-welded joints in steel structures will be recapitulated for reference purposes, considering the generalized random fatigue limit (GRFL) model (Chapter 2). Particular attention will be paid to the parameter estimate confidence bounds as well as quantile S_e-N curves for CA fatigue design. Collecting a large variety of VA fatigue test data from literature, a generalized random non-linear damage accumulation (GRNDA) model incorporating the response and resistance parts will be established to reveal the fatigue limit degradation and stochastic damage characteristics, based on a frequency domain approach (Chapter 3). Global mean stress effects will be investigated as well. CA-VA fatigue resistance similarity, i.e. VA data fitting the CA data scatter band will be verified, and damage reliability levels as well as confidence bounds will be evaluated. D values for design will be provided and compared to the recommended ones from guidelines and codes.

2. Constant amplitude fatigue

The effective notch stress S_e as the fatigue strength parameter will be introduced first (Section 2.1), to obtain one S_e-based CA MCF and HCF resistance data scatter band for all arc-welded joints in steel structures. A GRFL model will be established, and particular attention will be paid to the fatigue lifetime and fatigue limit distributions providing the best fit, the most likely parameter estimates and confidence bounds, as well as the quantiles to be used for fatigue design (Section 2.2).

2.1. Effective notch stress parameter

Through-thickness weld notch stress distributions are assumed to be a key element for an appropriate fatigue design criterion. Semi-analytical formulations $\sigma_n(r/t_p)$, with plate thickness t_p either the base plate or cross/connection/cover plate value, t_b or t_c (Figures 1 and 6), have been developed for both non-symmetry and symmetry with respect to half the plate thickness ($t_p/2$), in case of both zero and finite notch radius ρ (Qin et al. 2019; Bufalari et al. 2024). Typically, three zones can be identified in all distributions: the zone 1 peak stress value (Figure 1, red), the zone 2 notch-affected stress gradient (Figure 1, white), and the zone 3 far-field dominated stress gradient (Figure 1, blue), demonstrating stress field similarity (Den Besten 2015).

Since the (as) weld(ed) ρ value is typically small, a zone 1 peak stress fatigue strength parameter would be too conservative. Embedded in the critical distance theory (Taylor 2008), an effective notch stress estimate σ_e can be obtained by averaging $\sigma_n(r/t_p)$ along the expected crack path over a material characteristic micro- and meso-structural length $\rho^\star$ (Figure 1); another mechanism contribution – rather than introducing a fictitious notch radius (e.g. Sonsino et al. 2012; Zhang et al. 2012; Radaj et al. 2013), partially incorporating a zone 2 notch stress gradient and zone 3 far field stress gradient contribution as well. Physically speaking, $\rho^\star$ reflects the length along which the majority of the fatigue damage has accumulated.

A complete spatial description of a mechanical loading-induced response cycle requires two parameters to be involved. The range S_e and the ratio $R = (S_{e,min}/S_{e,max})$ are selected for this purpose. Walker's mean stress model (Walker 1970) typically provides the best results for welded joints (Qin et al. 2021; Bufalari et al. 2024)

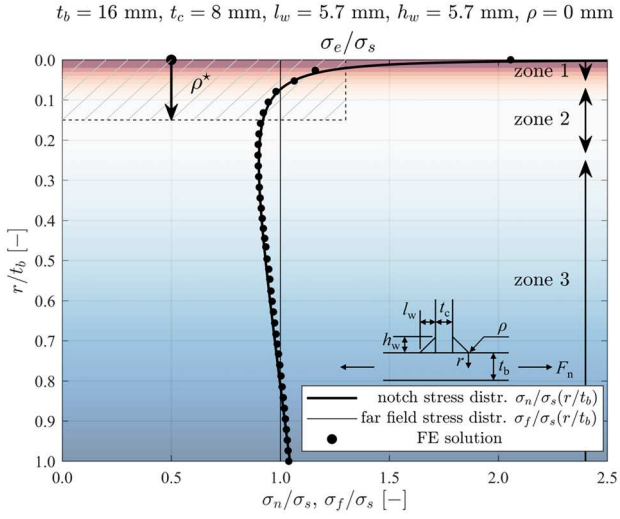

Figure 1. Through-thickness weld notch stress distribution in a T-joint used to calculate the averaged effective notch stress (Equation 1). (This figure is available in color online.)

and the effective notch stress parameter becomes:

$$S_e(\rho^*, \gamma) = \Delta\sigma_e = \frac{\frac{t_p}{\rho^*}\int_0^{\frac{\rho^*}{t_p}}\left\{\sigma_n\left(\Delta\sigma_s, \frac{r}{t_p}\right)\right\}d\left(\frac{r}{t_p}\right)}{(1-R)^{1-\gamma}}. \quad (1)$$

The exponent γ is a fitting parameter and reflects another strength contribution, implicitly incorporating the mean welding-induced residual stress as well. For $\gamma \to 1$, the range dominates the fatigue resistance; the ratio becomes governing for $\gamma \to 0$.

2.2. Resistance formulation

Fatigue requires a driving force to turn an intact geometry into one containing cracks (e.g. den Besten 2018), implying a barrier or threshold may exist. Although for arc-welded joints, defects – random in number and size – virtually eliminate the crack nucleation part of the damage process, the CA MCF to HCF fatigue resistance transition shows an increasing slope and m even tends to become infinitely large, introducing a fatigue limit, a stochastic variable $S_\infty(\mu, \sigma)$ as incorporated in the random fatigue limit model (Leonetti et al. 2017). Using $S_e(\rho^\star, \gamma)$ as fatigue strength parameter, a GRFL resistance curve formulation at a base 10 log-scale can be obtained for all arc-welded joints in steel structures (Qin et al. 2021):

$$\log(N) = \log(C) - m \cdot \log\{S_e(\rho^*, \gamma)\} - \rho_{S_\infty} \cdot \log\left\{1 - \frac{S_\infty(\mu, \sigma)}{S_e(\rho^*, \gamma)}\right\}. \quad (2)$$

Although fatigue limit behaviour will remain a hypothesis anyway and difficult to prove, the GRFL model (Equation 2) provides statistically the most accurate fatigue strength and lifetime estimates (Qin et al. 2021).

To be able to incorporate both complete and right-censored data, i.e. failures and run-outs, Maximum Likelihood regression at natural log-scale is adopted to obtain the parameter estimates:

$$\max_{\theta_{CA}}\left[\mathcal{L}\{\theta_{CA}; N|S_e(\rho^*, \gamma)\}\right] \quad (3)$$

with likelihood

$$\mathcal{L}\{\theta_{CA}; N \mid S_e(\rho^*, \gamma)\} = \sum_{i=1}^{n}\Big[\delta_i \ln f(N_i \mid S_{e,i}(\rho^*, \gamma); \theta_{CA}) + (1-\delta_i)\ln\left(1 - F(N_i \mid S_{e,i}(\rho^*, \gamma); \theta_{CA})\right)\Big].$$

data-type indicator

$$\delta_i = \begin{cases} 0 & \text{for a failure} \\ 1 & \text{for a run-out} \end{cases}$$

and parameter vector

$$\theta_{CA} = \{\ln(C),\ \gamma, m, \rho^*, \sigma_N, \rho_{S_\infty}, S_{\infty,\mu}, S_{\infty,\sigma}\}.$$

The marginal joint probability density function f(.) and corresponding cumulative distribution function F(.) for N and S_∞ relating to the MCF finite and HCF infinite lifetime region denote:

$$f(N_i|S_{e,i}(\rho^*, \gamma); \theta_{CA}) = \int_0^{S_{e,i}}\{f(N_i|S_{e,i}(\rho^*, \gamma); \mu_N, \sigma_N)\cdot f(x; S_{\infty,\mu}, S_{\infty,\sigma})\}dx \quad (4)$$

and

$$F(N_i|S_{e,i}(\rho^*, \gamma); \theta_{CA}) = \int_0^{S_{e,i}}\{F(N_i|S_{e,i}(\rho^*, \gamma); \mu_N, \sigma_N)\cdot f(x; S_{\infty,\mu}, S_{\infty,\sigma})\}dx \quad (5)$$

with

$$\mu_N = \ln(C) - m\cdot\ln\{S_{e,i}(\rho^*, \gamma)\} - \rho_{S_\infty} \cdot \ln\left\{1 - \frac{\exp(x)}{S_{e,i}(\rho^*, \gamma)}\right\}.$$

The integral upper bound being $S_{e,i}$ rather than ∞ may suggest that a part of the domain is excluded since $S_\infty < S_{e,i}$ does not necessarily hold for each fatigue test result. However, estimating $S_\infty > S_{e,i}$ for a single data point has no physical meaning. At the same time, from a mathematical point of view, the integral operators (Equations 4 and 5) are undefined for $\exp(x)/S_{e,i} > 1$. The same reasoning holds for the integral lower bound being 0 rather than $-\infty$.

A Normal-distributed lifetime N typically provides the best fit (Qin et al. 2021), meaning:

$$f(N_i|S_{e,i}(\rho^*, \gamma); \mu_N, \sigma_N) = \frac{1}{\sqrt{2\pi}\cdot\ln(10^{\sigma_N})}\cdot\exp\left[-\frac{\{\ln(N_i) - \mu_N\}^2}{2\cdot\ln(10^{\sigma_N^2})}\right] \quad (6)$$

and

$$F(N_i|S_{e,i}(\rho^*, \gamma); \mu_N, \sigma_N) = \frac{1}{2}\left[1 + \mathrm{erf}\left\{\frac{\ln(N_i) - \mu_N}{2\cdot\ln(10^{\sigma_N})}\right\}\right]. \quad (7)$$

For the fatigue limit, a weakest-link formulation is more appropriate (Qin et al. 2021), introducing an Extreme

Value type-I (minimum) distribution (Gumbel 1954) with mean $S_{\infty,\mu}$, standard deviation $S_{\infty,\sigma}$, and Euler constant γ_E:

$$f(x;\, S_{\infty,\mu},\, S_{\infty,\sigma}) = \left\{\frac{1}{\left(\frac{\sqrt{6}}{\pi}\right)\ln\left(S_{\infty,\sigma}\right)}\right\} \cdot \exp\left[\frac{x-\left(\ln\left(S_{\infty,\mu}\right)+\left(\frac{\sqrt{6}}{\pi}\right)\ln\left(S_{\infty,\sigma}\right)\gamma_E\right)}{\left(\frac{\sqrt{6}}{\pi}\right)\ln\left(S_{\infty,\sigma}\right)} - \exp\left\{\frac{x-\left(\ln\left(S_{\infty,\mu}\right)+\left(\frac{\sqrt{6}}{\pi}\right)\ln\left(S_{\infty,\sigma}\right)\gamma_E\right)}{\left(\frac{\sqrt{6}}{\pi}\right)\ln\left(S_{\infty,\sigma}\right)}\right\}\right]. \quad (8)$$

The natural logarithm-based likelihood regression (Equation 3) is adopted because of the exp(·) operators appearing in the probability density functions (Equations 6 and 8). Note that a Normal distribution on a logarithmic scale corresponds to a log-Normal distribution at a linear scale (Equations 2, 6 and 7). Similarly, the Extreme Value distribution type-I turns into a Weibull one.

Applying Maximum Likelihood regression to CA fatigue test data of arc-welded joints in steel structures (sample size ~ 3000), the most likely parameter vector estimate $\hat{\theta}_{CA}$ is obtained (Table 1) including parameter confidence bounds based on likelihood ratio tests, as well as the normalized covariance matrix (Table 2). Different geometries, e.g. butt-joints, T-joints, cruciform joints, attachments, cover plates, gusset plates, etc. are involved, with plate thickness t_p ranging from 2 to 160 mm. The mean stress levels are different from one data series to another as reflected in $R = -1$ to 0.8 (Qin et al. 2021).

The log–log linear MCF behavior (Equation 2) explains a highly correlated intercept $\log(C)$ and slope m (Table 2). Note that the m estimate is close to the typical design value $m = 3$ (e.g., Hobbacher and Baumgartner 2024). Confidence of the MCF parameters {$\log(C)$, γ, m, ρ^*, σ_N} turns out to be high (Table 1) because of the significant amount of resistance data involved. Walker's most likely mean stress exponent γ indicates a stress range contribution close to 90% of the effective stress value (Table 1). The remaining 10% reflects a mean stress effect and incorporates both the welding residual as well as the mechanical response-induced component, providing a relatively small but non-negligible contribution as reflected in the $\log(C)$-γ strength parameter correlation (Table 2). A most likely $\rho^* \sim 1$ mm (Table 1) suggests that the majority of the fatigue damage is accumulated in the notch-affected region indeed. The m-ρ^* mechanism parameter correlation (Table 2) confirms an effective ρ^* contribution to the fatigue characterization of welded joints. Both the σ_N-γ and σ_N-ρ^* correlations (Table 2) show that mean stress and scaling are important for reducing the data scatter. The most likely σ_N estimate, on a base 10 log scale (Table 1), reflects an excellent S_e fatigue strength parameter performance, supporting one fatigue resistance curve for all arc-welded joints.

The {$S_{\infty,\mu}$, $S_{\infty,\sigma}$} parameter confidence (Table 1) reflects the relatively small amount of HCF resistance data containing predominantly run-outs. All $\rho_{S\infty}$ correlations (Table 2) indicate a key parameter role for $\rho_{S\infty}$ in relating MCF and HCF, showing the added value of the GRFL model. The most likely $\rho_{S\infty}$ (Table 1) suggests a gradual MCF to HCF transition. Last but not least, the large ρ^*-{$S_{\infty,\mu}$, $S_{\infty,\sigma}$} correlation seems to support distinct MCF and HCF ρ^* values, rather than an average (constant) one for the combined regions.

Table 1. GRFL model's most likely parameter estimates (MLE's), including 95% lower and upper confidence bounds (LCB and UCB).

parameter	log(C)	γ	m	ρ*	σN	ρS∞	S∞,μ	S∞,σ
LCB0.95	12.96	0.86	3.02	1.11	0.21	0.30	72	45
MLE	13.14	0.88	3.08	1.17	0.22	0.42	84	50
UCB0.95	13.32	0.90	3.14	1.23	0.23	0.56	97	54

Table 2. GRFL model's parameter normalized covariance matrix.

parameter	log(C)	γ	m	ρ*	σN	ρS∞	S∞,μ	S∞,σ
log(C)	1	0.118	0.867	0.101	0.365	−0.554	0.260	−0.136
Γ		1	0.128	−0.336	0.118	−0.326	−0.208	0.352
m			1	−0.235	0.293	−0.801	−0.026	0.232
ρ*				1	0.171	0.514	0.913	−0.869
σN					1	−0.289	0.340	−0.225
ρS∞						1	0.181	−0.453
S∞,μ							1	−0.874
S∞,σ								1

The most likely parameter vector $\hat{\theta}_{CA}$ can be used to establish fatigue resistance quantiles $N(S_e)$. A particular probability of survival p_s is required to ensure a sufficient level of reliability, as well as an assigned level of confidence c_l to deal with the fatigue resistance induced uncertainties, in order to establish a design curve $R(p_s)C(c_l)$. The RFL model requires implicit solutions for $N(S_e)$ in the MCF and HCF regions:

$$F(N|S_e;\, \hat{\theta}_{CA}) = F(N|S_e;\, \hat{\mu}_N,\, \hat{\sigma}_{N,cl}) = (1 - p_s). \qquad (9)$$

The fatigue limit mean (p_s ~0.43), median (p_s ~0.50), and mode (p_s ~0.63) show the $S_\infty(\mu,\ \sigma)$ behavior when shifting from MCF to HCF (Figure 2). However, R99C90 for design shows approximately single slope behaviour because of the relatively low $S_\infty(\mu,\ \sigma)$ reliability and confidence.

Rather than a GRFL model, IIW guidelines (Hobbacher and Baumgartner 2024) and codes (e.g. British Standard 2014; DNV 2024; CEN 2025) typically adopt a bi-linear one to formulate the CA fatigue resistance, providing a finite slope in the HCF region. Although typically piecewise continuous, a continuous formulation (Qin et al. 2021) may be preferred to improve the numerical stability for Maximum Likelihood regression:

$$\begin{aligned}\log(N) = {} & \log(C) - m_{MCF} \cdot \log\{S_e(\rho^*,\ \gamma)\} \\ & - \left(\frac{m_{MCF}}{m_{HCF}} - 1\right) \\ & \cdot \log\{1 + \exp[\log\{S_e(\rho^*,\ \gamma)\} - \log(S_t)]^{-m_{HCF}}\}.\end{aligned} \qquad (10)$$

For the effective notch stress beyond the transition value, $\{S_e(\rho^*,\ \gamma) > S_t|N_t\}$, the MCF slope m_{MCF} is in charge; for $\{S_e(\rho^*,\ \gamma) \le S_t|N_t\}$, the HCF one m_{HCF}. Initially adopting the parameter vector $\theta_{CA} = \{\ln(C),\ \gamma,\ m_{MCF},\ \rho^*,\ S_t,\ m_{HCF},\ \sigma_N\}$, the lifetime standard deviation σ_N covers the full MCF-HCF region (case 1). However, the test data shows a natural increase in lifetime scatter, motivating the introduction of separate MCF and HCF statistical distributions. Assuming that the material characteristic length and mean stress effects hardly change when shifting from MCF to HCF, the parameter vector turns into: $\theta_{CA} = \{\ln(C),\ \gamma,\ m_{MCF},\ \rho^*,\ \sigma_{N,MCF},\ S_t,\ m_{HCF},\ \sigma_{N,HCF}\}$. A Normal-distributed lifetime N typically provides the best fit for the MCF region (Qin et al. 2021) and could be extended to the HCF one (case 2), but an Extreme Value type-I (maximum) distribution (Gumbel 1954) may better reflect the weakest link nature of the HCF region (case 3).

Maximum Likelihood regression analysis results for all three cases (Table 3, Figures 3–5) show a similar m_{MCF} ~3.4 estimate, beyond the common $m = 3$ like obtained for the GRFL model (Table 1, Figure 2) as well, but the same value as identified for high-quality butt joints only (Mehmanparast et al. 2024) and adopted in a recent code slope change (DNV 2024; Lotsberg 2025). The main reason explaining the difference seems to be the gradual MCF-HCF transition as naturally included in the GRFL model (Equation 2) and the piecewise continuous one in the bi-linear model (Equation 10), affecting the m_{MCF} estimate. The HCF slope estimates differ from one case to another – i.e. considering distinct MCF and HCF lifetime statistics or not and the adopted lifetime distribution – and are correlated to the most likely transition point: for increasing $S_t|N_t$, $m_{HCF} \to m_{MCF}$. One σ_N for the full MCF-HCF range (case 1) provides $m_{HCF} \approx 5$ with high parameter confidence, a value adopted in some codes as well (e.g. CEN 2025), but way below $m_{HCF} = 22$ as suggested in the IIW guidelines (e.g. Hobbacher and Baumgartner 2024) or even $m_{HCF} \to \infty$, reflecting a CA fatigue limit, as used in other codes (e.g. British Standard 2014; DNV 2024; Johnston and Horn 2024). The most likely transition at $S_t|N_t \approx 1{\cdot}10^7$ cycles is the same as is often used for design (e.g. British Standard 2014; DNV 2024; Hobbacher and Baumgartner 2024). Distinguishing MCF and HCF Normal lifetime distributions (case 2), $m_{HCF} \sim 5$, but an Extreme Value distribution in the HCF region (case 3) provides $m_{HCF} \to m_{MCF}$ and comes along with an improved statistical performance, as reflected in the Akaike Information Criterion (AIC) relative to the GRFL model. The most likely MCF-HCF transition location shifted to $S_t|N_t \approx 2{\cdot}10^6$ and $S_t|N_t \approx 1{\cdot}10^6$ cycles, respectively, and is in agreement with the recent trend to move the transition to a smaller number of cycles in the codes (e.g. DNV 2024; CEN

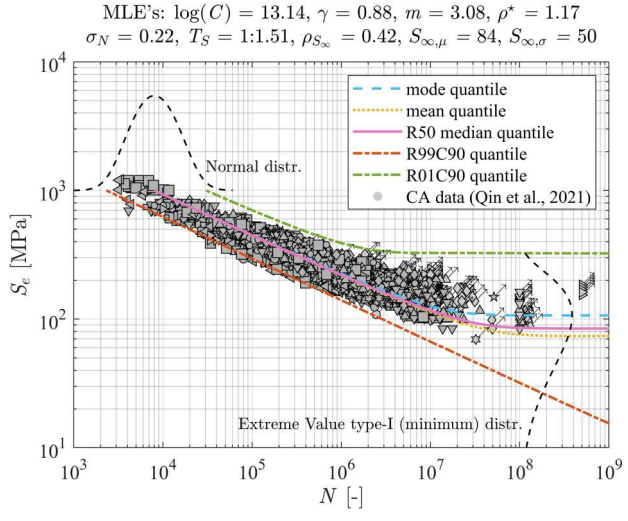

Figure 2. S_e-based CA MCF and HCF resistance formulation using a GRFL model. (This figure is available in color online.)

Table 3. Bi-linear model MLE's for three cases, including 95% LCB and UCB as well as the relative AIC.

	parameter	log(C)	γ	m_{MCF}	ρ*	σ_N / $\sigma_{N,MCF}$	S_t | N_t	m_{HCF}	$\sigma_{N,HCF}$	rel. AIC
Normal	$LCB_{0.95}$	13.99	0.84	3.35	1.03	0.28	121	5.57	-	1.27
	MLE	14.14	0.86	3.43	1.09	0.29	121 | $1{\cdot}10^7$	5.68	-	
	$UCB_{0.95}$	14.29	0.88	3.50	1.13	0.30	122	5.78	-	
Normal / Normal	$LCB_{0.95}$	13.72	0.85	1.91	1.11	0.24	186	4.35	0.53	1.14
	MLE	13.90	0.86	3.34	1.12	0.25	188 | $2{\cdot}10^6$	4.69	0.56	
	$UCB_{0.95}$	14.33	0.87	4.78	1.13	0.26	189	5.41	0.60	
Normal / EV-type I maximum	$LCB_{0.95}$	14.08	0.86	3.42	1.16	0.23	231	3.57	0.34	1.07
	MLE	14.16	0.87	3.45	1.17	0.24	232 | $1{\cdot}10^6$	3.7	0.38	
	$UCB_{0.95}$	14.23	0.88	3.48	1.18	0.24	236	3.82	0.40	

2025). However, this shift may significantly impact the VA fatigue assessment.

A single MCF-HCF lifetime standard deviation (case 1) provides $\sigma_N \sim 0.29$ and is relatively large in comparison to the GRFL model estimate (Table 1) as a result of the HCF lifetime scatter (Figures 2–5). Distinct MCF and HCF lifetime distributions (cases 2 and 3) show $\sigma_{N,MCF} \sim 0.25$ and $\sigma_{N,HCF} \sim 0.24$, respectively, reflecting an improvement with respect to the single MCF-HCF σ_N, but still relatively large in comparison to the GRFL value (Table 1) since a joint probability density (Equations 4 and 5) is not included. The respective $\sigma_{N,HCF} \sim 0.56$ and $\sigma_{N,HCF} \sim 0.38$ estimates clearly indicate the large HCF resistance lifetime scatter and an Extreme Value distribution (case 3) providing a better fit.

The modeling choices as reflected in the three cases have consequences for the fatigue design R99C90 quantiles (Figures 3–5). Although one MCF-HCF lifetime standard deviation (case 1) may cause unnecessarily conservative MCF lifetime estimates, the relatively large amount of MCF data is statistically dominant and prevents this to a large extent.

Separate MCF and HCF lifetime distributions (cases 2 and 3) principally provide design quantiles containing a transition step because of distinct $\sigma_{N,MCF}$ and $\sigma_{N,HCF}$. An engineering solution might be to extend the MCF part up to the HCF intersection,

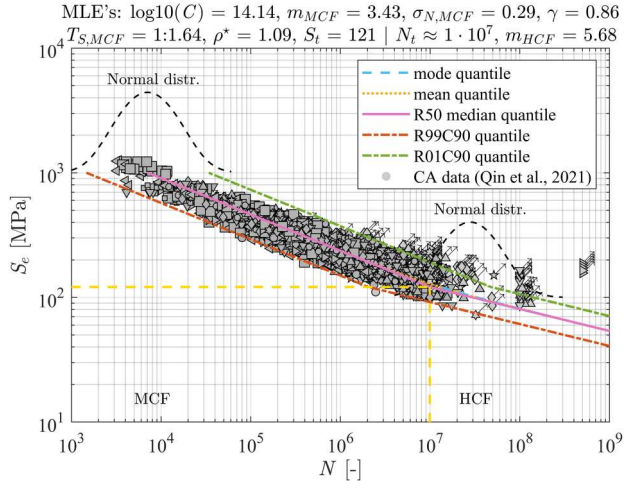

Figure 3. S_e-based CA MCF and HCF resistance formulation using a bi-linear model with one MCF-HCF statistical lifetime distribution (case 1). (This figure is available in color online.)

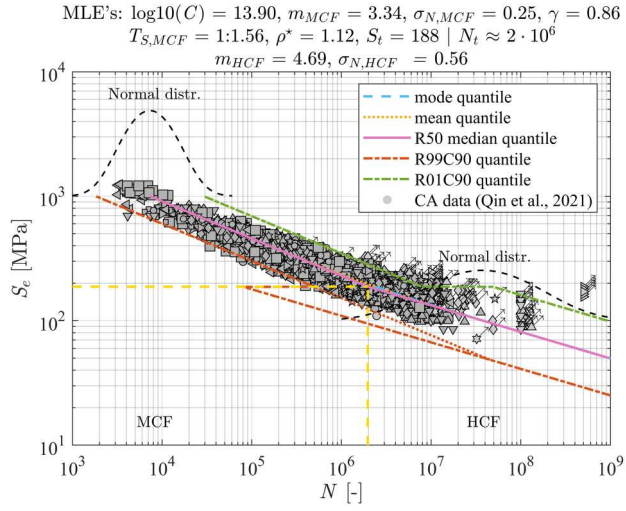

Figure 4. S_e-based CA MCF and HCF resistance formulation using a bi-linear model with distinct MCF and HCF statistical lifetime distributions (case 2). (This figure is available in color online.)

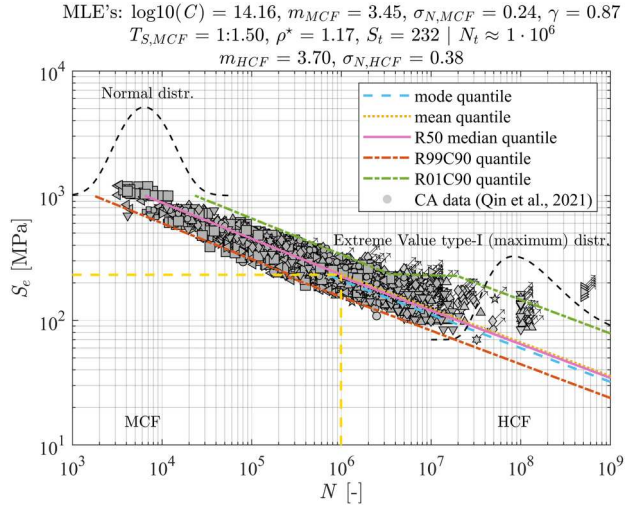

Figure 5. S_e-based CA MCF and HCF resistance formulation using a bi-linear model with distinct MCF and HCF lifetime statistical distributions (case 3). (This figure is available in color online.)

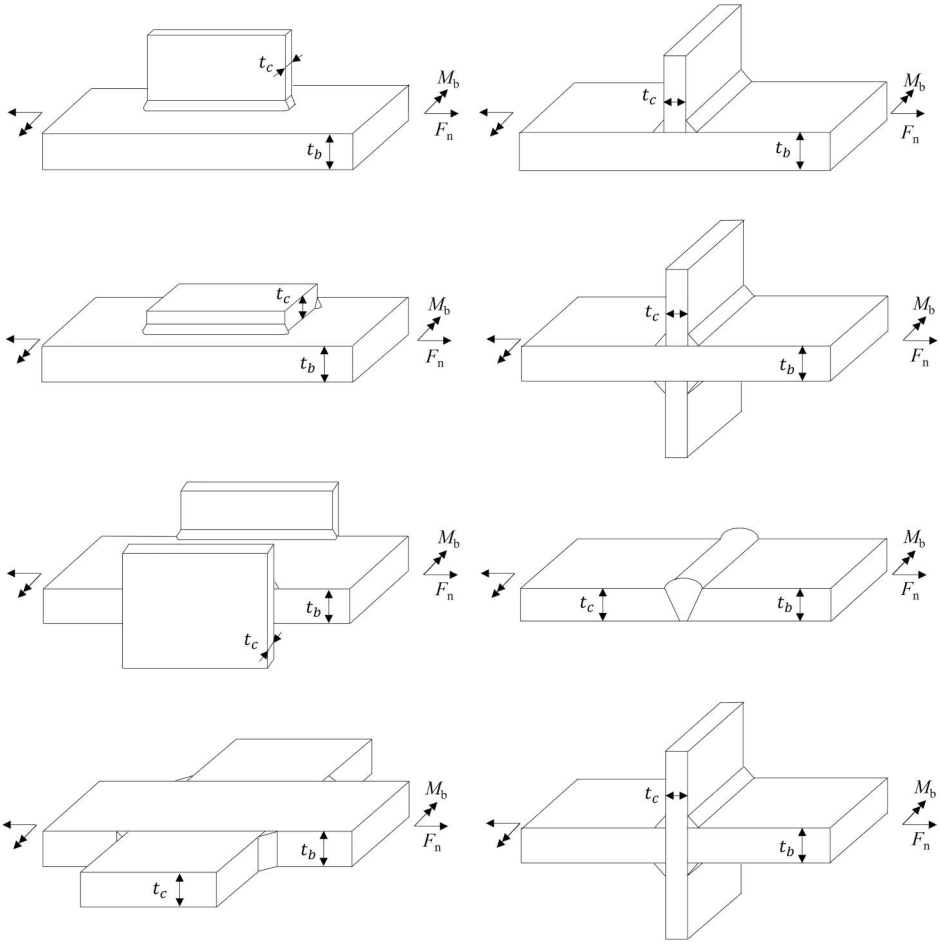

Figure 6. Specimen geometries for VA fatigue test data from literature; hot spot type A (a, c), type B (e, g), and type C (b, d, f, h). (This figure is available in color online.)

but this compromises the reliability and confidence level of the lifetime estimates locally, in particular for the Normal lifetime distributions (case 2). The MCF-HCF transition location shifts to $S_t|N_t \approx 3{\cdot}10^7$ cycles (Figure 3), close to $S_t|N_t \approx 5{\cdot}10^7$ (British Standard 2014). Since $m_{HCF} \rightarrow m_{MCF}$ for an HCF Extreme Value lifetime distribution (case 3) – the best performing bi-linear model – the design quantile is basically a single slope curve (Figure 4), like for the GRFL model (Figure 2). However, the relative AIC = 1 value indicates that the GRFL model provides overall the best statistical performance, explaining why this one is adopted as starting point for VA fatigue modeling.

3. Variable amplitude fatigue

Aiming for CA-VA resistance similarity in the MCF and HCF regions, to obtain accurate VA fatigue lifetime estimates adopting a frequency domain approach, VA fatigue test data from literature for arc-welded joints in steel structures has been collected first (Table 4). The sample (size ~ 480) includes butt-joints, T-joints, cruciform joints, attachments, gusset plates and cover plates (Figure 6). Plate thickness t_p ranges from 6 to 30 mm. The applied loading is a cyclic normal force F_N or bending moment M_b. About 10 different types of spectra are involved, ranging from small to wide band, and from block loading to storm loading conditions. Hot spots type A, B and C (Fricke 2012) are observed; ~140, ~40 and ~300 specimens, implying respectively fatigue cracks at a weld end in plate thickness direction, edge cracks at a weld end and cracks along the weld seam in plate thickness direction. The maximum hot spot structural stress $S_{h,max}$ based data presentation (Figure 7), as typically used to establish a Gassner curve (Chapter 1), clearly indicates the lack of CA-VA fatigue resistance similarity. The weld notch stress distribution $\sigma_n(r/t_p)$ and the effective notch stress S_e (Equation 1) as required for analysis are verified using solid finite element models and linear elastic analyses providing converged solutions (e.g. Figure 1).

Table 4. VA fatigue database.

source	steel grade	hot spot type	Joint type (Figure 6)	t_p [mm]	loading distribution
Schilling et al. 1978	A514	A	c	9.5	Rayleigh
Albrecht and Friedland 1979	A588	C	d	10	measurement replica
Albrecht et al. 1979	A589	C	d	10	measurement replica
Fisher et al. 1983	A514	C, A	d, c	16; 9.5	Rayleigh
Klippstein and Schilling 1989	A572	C	d	9.5	Rayleigh
Ota et al. 1997	SPV50	C	f	20	Rayleigh
Rörup and Petershagen 1999	ST 52–3	A	a	12.5	log-linear
Agerskov 2000	ST. 52–3	C	d	16, 8	Broad 64, Pierson-Moskowitz
Demofonti et al. 2001	S355, S960Q	C	f, d	10, 30	Gauss, Gauss overloads
Zhang and Maddox 2009	BS 4360	B, A	e, a	12; 12.5	linear
Baptista et al. 2017	S235JR	B	g	15	block
Yıldırım et al. 2020	AH36, S690QL	C	d	6	log-linear
Braun et al. 2022	-	C	f	10	slamming
Deul 2021	S355	C	d	25	Rayleigh
Duan et al. 2023	Q345B	C	h, b	8; 16	block
Leonetti et al. 2024	S690QL	C	d	10	measurement replica

To reveal the CA fatigue limit degradation and non-linear damage accumulation characteristics for VA conditions, the GRNDA model parameters (Section 3.1) incorporating response and resistance parts will be established using S_e as fatigue strength parameter (Section 2.1). VA test data fitting the CA data scatter band (Section 2.2) – reflecting fatigue resistance similarity – will be verified (Section 3.1). Damage reliability levels as well as confidence bounds will be evaluated in comparison to recommended D values for design (Section 3.2).

3.1. Damage accumulation model

Fatigue is a progressive damage process. The damage rate, i.e. the damage per cycle, is defined as $\dot{D} = \left(\mathrm{D}/\sum \mathrm{n_j}\right)$. Using the linear damage accumulation model, the rate formulation turns into $\dot{D} = \sum (n_j/N_j)/\sum n_j$. At the same time $\sum n_j = (D/\dot{D})$, meaning for each fatigue specimen the lifetime estimate becomes:

$$N_i = \int \left(\frac{D}{\dot{D}}\right) \mathrm{d}D \approx \sum_{h=1}^{h_{tot}} \left(\frac{D_h}{\dot{D}}\right) = \sum_{h=1}^{h_{tot}} \left[\frac{\frac{D(\mu,\,\sigma)}{h_{tot}}}{\sum_j \left\{ \frac{1}{N_j} \cdot \frac{n_j}{\sum (n_j)} \right\}} \right]. \quad (11)$$

Note the damage rate is different from a similar formulation (Leonetti et al. 2020), as $\dot{D}$ is defined per cycle rather than per total number of cycles in the response spectrum $\sum n_j$. In addition, a stochastic damage $D(\mu, \sigma)$ is adopted and replaces the constant one (Equation 11). The number of cycles N_j for each spectral bin reflects the CA GRFL information (Equation 2), providing a resistance-induced damage non-linearity:

$$N_j = 10^{\log(C) - m \cdot \log(S_{e,j}) - \rho_{S_\infty} \cdot \log\left\{ \frac{S_{\infty,VA}(D_h)}{S_{e,j}} \right\}}. \quad (12)$$

The VA conditions are assumed not to affect the CA-based strength and mechanism parameters {log(C), γ} and {m, $\rho^\star$}, but a VA equivalent fatigue limit is introduced (Leonetti et al. 2020), incorporating a damage history D_h-dependent degradation up to step h:

$$S_{\infty,VA}(D_h) = S_\infty(\mu,\,\sigma) \cdot \left\{ 1 - \frac{D_h}{D(\mu,\,\sigma)} \right\}^{\zeta}. \quad (13)$$

For increasing D, the fatigue limit decreases, meaning the damage accumulation calculation becomes an iterative process. Damage exponent ζ reflects the response induced non-linearity – either convex or concave downward (Figure 8).

Involving the fatigue strength parameter S_e rather than the nominal or hot spot structural stress range, respectively S_n or S_h, allows for a generalized formulation – one resistance curve for all arc-welded joints

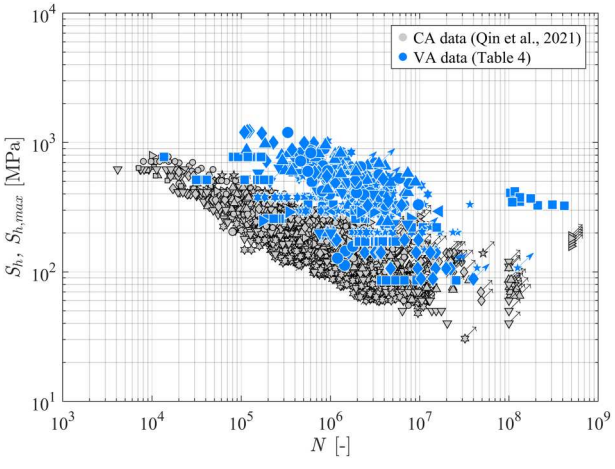

Figure 7. Hot spot structural stress range based comparison of CA and VA test data using S_h and $S_{h,max}$, respectively. (This figure is available in color online.)

in steel structures – to estimate the VA model parameters with high confidence. Maximum Likelihood regression at natural log-scale is adopted to obtain the parameter estimates:

$$\max_{\theta_{VA}} \{\mathcal{L}(\theta_{VA}; N|\{S_{e,j}\}_i)\} \tag{14}$$

with likelihood

$$\mathcal{L}(\theta_{VA}; N|\{S_{e,j}\}_i) = \sum_{i=1}^{n} [\delta_i \cdot \ln\{f(N_i|\{S_{e,j}\}_i; \theta_{VA})\} + (1-\delta_i) \cdot \ln\{1 - F(N_i|\{S_{e,j}\}_i; \theta_{VA})\}],$$

parameter vector

$$\theta_{VA} = \{\sigma_{N,VA}, D_\mu, D_\sigma, \zeta\}$$

and for each specimen i, the involved effective notch stress spectrum:

$$\{S_{e,j}\}_i = \{S_{e,1}, \ \ldots, \ S_{e,k}\}_i.$$

The marginal joint probability density function f(.) and corresponding cumulative distribution function F(.) for N and D denote:

$$f(N_i|\{S_{e,j}\}_i; \theta_{\mathrm{VA}}) = \int_0^\infty \{f(N_i|\{S_{e,j}\}_i; \mu_{N,VA}, \sigma_{N,VA}) \cdot f(x; D_\mu, D_\sigma)\}\mathrm{d}x \tag{15}$$

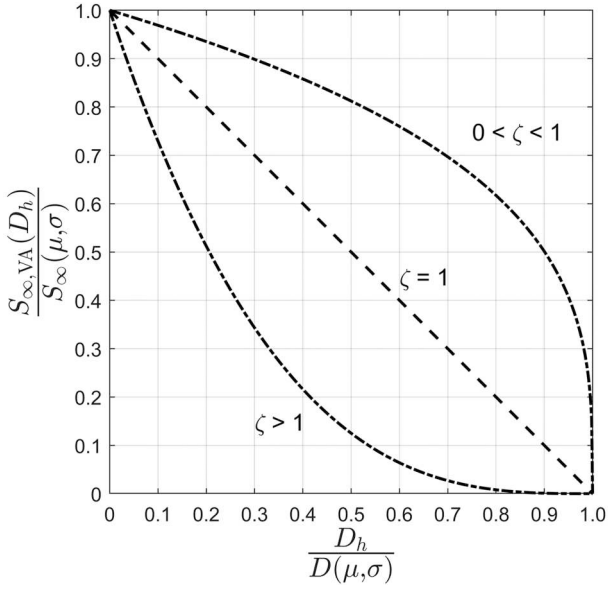

Figure 8. Fatigue limit degradation for different ζ values. (This figure is available in color online.)

and

$$F(N_i|\{S_{e,j}\}_i; \theta_{\mathrm{VA}}) = \int_0^\infty \{F(N_i|\{S_{e,j}\}_i; \mu_{N,VA}, \sigma_{N,VA}) \cdot f(x; D_\mu, D_\sigma)\}\mathrm{d}x \tag{16}$$

with

$$\mu_{N,VA} = \sum_{\mathrm{h}=1}^{\mathrm{h_{tot}}} \left[\frac{\frac{\mathrm{x}}{\mathrm{h_{tot}}}}{\sum_{\mathrm{j}} \left\{ \frac{1}{\mathrm{N_j}} \cdot \frac{\mathrm{n_j}}{\sum(\mathrm{n_j})} \right\}} \right].$$

Since for lifetime $N(\mu, \sigma)$ a Normal distribution, provides the best fit:

$$f(N_i|\{S_{e,j}\}_i; \mu_{N,VA}, \sigma_{N,VA}) = \frac{1}{\sqrt{2\pi} \cdot \sigma_{N,VA}} \cdot \exp\left[-\frac{\{\ln(N_i) - \mu_{N,VA}\}^2}{2 \cdot \sigma_{N,VA}^2} \right] \tag{17}$$

and

$$F(N_i|\{S_{e,j}\}_i; \mu_{N,VA}, \sigma_{N,VA}) = \frac{1}{2}\left[1 + \mathrm{erf}\left\{ \frac{\ln(N_i) - \mu_{N,VA}}{2 \cdot \sigma_{N,VA}} \right\} \right]. \tag{18}$$

The same distribution is adopted for the lifetime dependent damage $D(\mu, \sigma)$:

$$f(x; D_\mu, D_\sigma) = \frac{1}{\sqrt{2\pi} \cdot D_\sigma} \cdot \exp\left[-\frac{\{x - D_\mu\}^2}{2 \cdot D_\sigma^2} \right]. \tag{19}$$

To verify if VA test data fits the CA data scatter band, an equivalent effective stress $S_{\mathrm{e,eq}}$ parameter is required and can be solved for equating the CA and VA lifetime formulations (Equations 2 and 10–12):

$$\exp\left[\ln(C) - m \cdot \ln(S_{e,eq}) - \rho_{S_\infty} \cdot \ln\left\{ \frac{S_\infty(\mu, \sigma)}{S_{e,eq}} \right\} \right] = \sum_{h=1}^{h_{tot}} \left[\frac{\frac{D(\mu, \sigma)}{h_{tot}}}{\sum_j \left\{ \frac{1}{N_j} \frac{n_j}{\sum(n_j)} \right\}} \right]. \tag{20}$$

Although the expected VA lifetime and damage estimates are not necessarily independent, $\{\sigma_{\mathrm{N,VA}}, D_\sigma\}$ most likely serve the same purpose. Following the linear nature of the expected N and D values, $\mathrm{E}[N{\cdot}D] = \mathrm{E}[N]{\cdot}\mathrm{E}[D] = D_\mu^2 \cdot f_{\sum h,j}(S)$, the lifetime and damage are uncorrelated (Dekking et al. 2005), meaning a single VA scatter and performance parameter can be introduced:

$$\sigma_{VA} = \sqrt{\sigma_{N,VA}^2 + D_\sigma^2}. \tag{21}$$

Table 5. GRNDA model's most likely parameter estimates (MLE's), including 95% lower and upper confidence bounds (LCB and UCB) without mean stress correction (top) and with mean stress correction (bottom).

parameter	D_μ	ζ	$\sigma_{N,VA}$
$LCB_{0.95}$	1.10	0.81	0.30
MLE	1.20	8.95	0.32
$UCB_{0.95}$	1.28	20.12	0.34
$LCB_{0.95}$	1.01	1.12	0.28
MLE	1.09	3.17	0.30
$UCB_{0.95}$	1.15	14.32	0.32

Table 6. GRNDA model's parameter normalized covariance matrix without mean stress correction (left) and with mean stress correction (right).

parameter	D_μ	ζ	$\sigma_{N,VA}$
D_μ	1	−0.945	0.894
ζ		1	−0.961
$\sigma_{N,VA}$			1
D_μ	1	−0.373	0.616
ζ		1	−0.882
$\sigma_{N,VA}$			1

VA data assessment – initially without mean stress effect using $\gamma = 1$ (Equation 1) – shows that a reasonable fit in the CA data scatter band is obtained (Figure 9), although about 10 different types of loading distributions are involved. The most likely D_μ (Table 5 left) is different from 1 and may be a result of influence factors not explicitly incorporated, like sequence effects (e.g. different in block loading and storm loading conditions) and mean stress. The VA scatter parameter σ_{VA} may seem relatively large, but corresponds to a CA equivalent VA lifetime scatter $\sigma_{N,VA}$ (Tables 1 and 7). A very similar $\sigma_{N,VA}$ and σ_N is, on the one hand, a coincidence, but shows at the same time that a similar lifetime scatter can be obtained for CA and VA using S_e as fatigue strength parameter, a GRFL resistance formulation and a GNRDA model. For verification purposes, assuming $\sigma_{N,VA} = \sigma_N$, D_σ turns out to compensate for obtaining the same σ_{VA} (Table 7), indeed, justifying the σ_{VA} formulation (Equation 21). Fatigue limit degradation exponent $\zeta >> 1$, implying a strong convex downward $S_{\infty,VA}$ degradation as soon as damage starts to accumulate. A log–log linear resistance curve formulation for VA fatigue, as often assumed (Hobbacher and Baumgartner 2024), seems reasonable. The ζ confidence turns out to be relatively low (Table 5 left) because of the very limited availability of $S_{e,eq}$-N HCF VA fatigue test data (Figure 9 left). The D_μ-ζ-$\sigma_{N,VA}$ correlation (Table 6, left) is quite large since all damage accumulation model parameters affect one-to-one the performance, as expected.

Mean stress affects the CA fatigue resistance (Chapter 2). A tensile one typically reduces the fatigue lifetime, whereas a compressive mean stress can increase N. Although for VA conditions in a time domain approach mean stress can be incorporated per cycle, this type of information is not available in the frequency domain. However, a global mean stress estimate can often be obtained, like the still water hogging/sagging condition for a ship structure. The estimates for the VA data are obtained by calculating the arithmetic mean S^g_{mean} of the VA loading-induced response $S_e(t)$

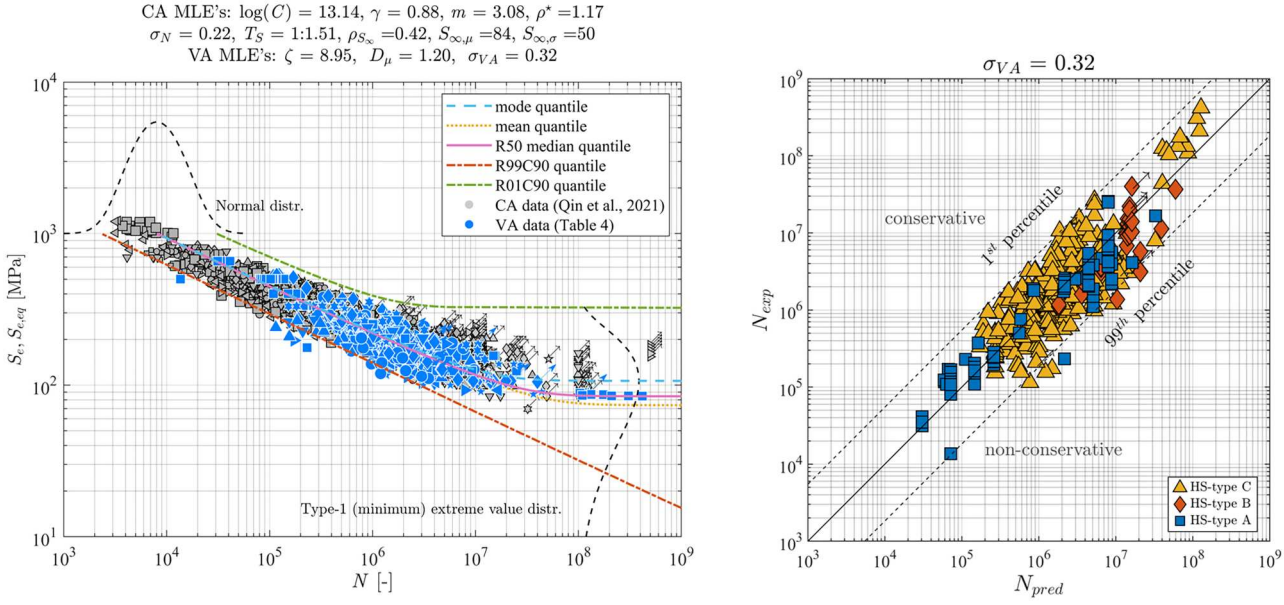

Figure 9. S_e-based VA MCF and HCF resistance formulation using a GRFL and GRNDA model without mean stress correction (left), predicted vs experimental lifetime N (right). (This figure is available in color online.)

Table 7: GRNDA model's lifetime and damage scatter

condition	σ_{VA}	$\sigma_{N,VA}$	D_σ
$\sigma_{N,VA}$ free	0.319	0.224	0.224
$\sigma_{N,VA} = \sigma_N$ assumption	0.319	0.220	0.229

signals providing a R_i for each spectral $S_{e,i}$:

$$R_i = \frac{S^g_{mean} - S_{e,i}/2}{S^g_{mean} + S_{e,i}/2}. \quad (22)$$

Incorporating the global mean stress, Maximum Likelihood regression provides a D_μ value one step closer to 1 in comparison to the results without global mean stress correction (Table 5, Figures 9 and 10). The VA scatter parameter σ_{VA} reduces accordingly from 0.32 to 0.30. Apparently, considering the global mean stress seems to be another step in the CA-VA fatigue resistance similarity direction. A significantly smaller ζ value is obtained, as well as a significant D_μ-ζ correlation reduction, suggesting the fatigue limit degradation exponent incorporates mean stress effects implicitly up to some extent.

However, one particular dataset (Rörup and Petershagen 1999) is excluded, containing a large number of fully compressive cycles with a global mean stress of −100 MPa, since the CA fatigue resistance data does not contain test results with $R > 1$ (Section 2.2) and the most likely γ does not apply. Ignoring the fully compressive cycles as a workaround, assuming that crack opening is required for mode-I damage accumulation seems a partial solution only, since the lifetime estimates tend to become non-conservative (Figure 11, right). Evaluating $R = -\infty$ CA data from the same source provides results outside the data scatter band. An additional residual stress component $S_{e,res}$ had to be incorporated: $R = (S_{e,min} + S_{e,res})/(S_{e,max} + S_{e,res})$ to shift the data into the scatter band, revealing that Walker's (exponential) mean stress model does not apply anymore for fully compressive response conditions: S_e is much less effective than estimated.

A ζ trend toward a more linear type of damage accumulation behavior is already observed (Table 5, Figures 9 and 10). Ignoring even the VA HCF data ($N \geq 10^8$), $\zeta \to \infty$ (Figure 12 left) suggests an instantaneous degradation of S_∞ to zero, and a log–log linear resistance formulation is sufficient as well when VA HCF is not relevant. Looking at the data distribution for the different types of loading distributions (Figure 12, right), a generalized formulation applicable for all arc-welded joints in steel (maritime) structures facing any VA loading and response condition seems to have been obtained indeed.

3.2. Critical damage estimates

One of the advantages of the presented CA GRFL resistance formulation and VA GRNDA model is that particular reliability and even confidence levels can be defined explicitly (Equation 24). Guidelines and codes (e.g. IIW, DNV, BS) typically use a log–log (bi-)linear resistance curve reflecting a certain reliability level and a LDA model. The maximum allowed damage is often established at $D = 0.5$ or D

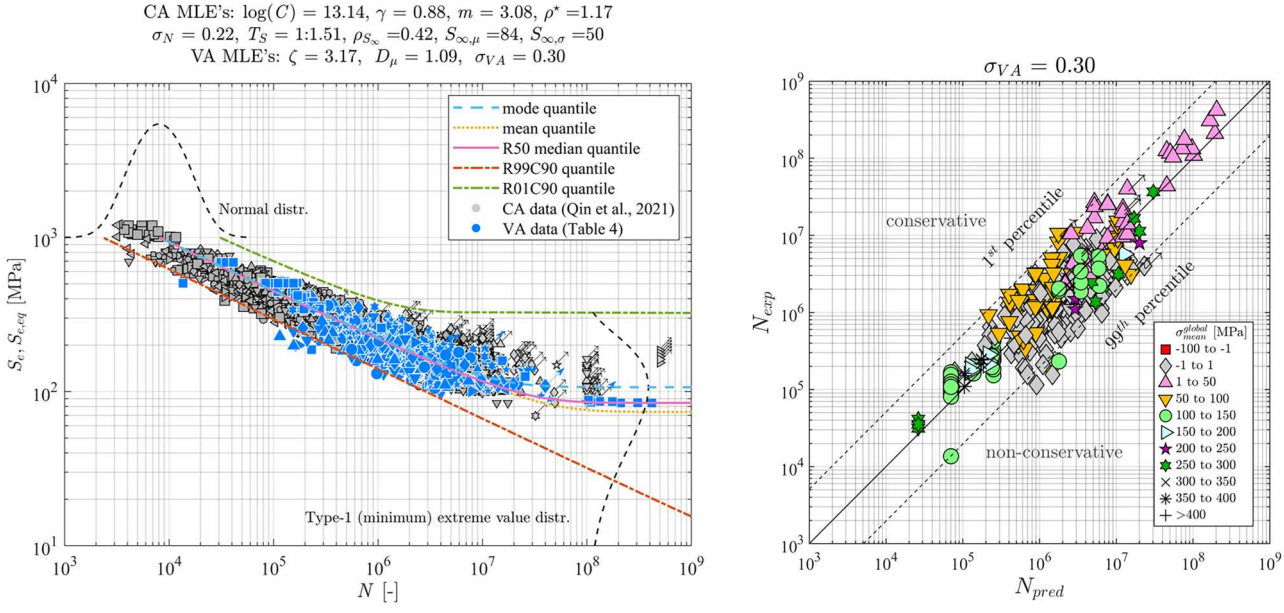

Figure 10. S_e-based VA MCF and HCF resistance formulation using a GRFL and GRNDA model with mean stress correction (left), predicted vs experimental lifetime N (right). (This figure is available in color online.)

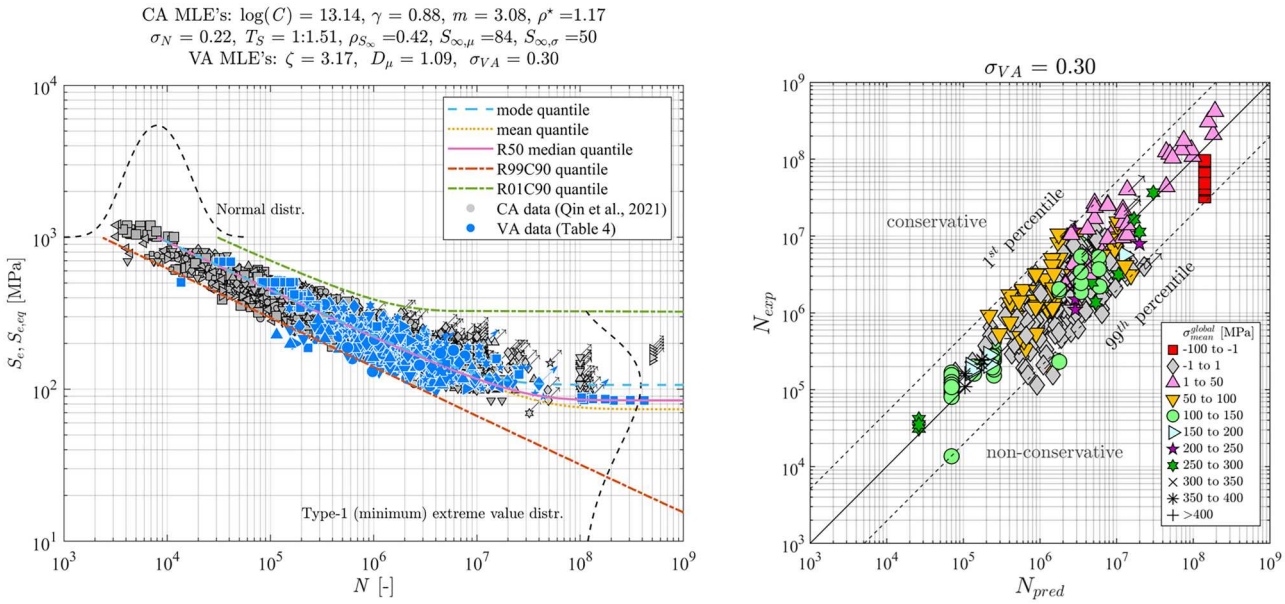

Figure 11. S_e-based VA MCF and HCF resistance formulation using a GRFL and GRNDA model with mean stress correction (left), predicted vs experimental lifetime N incl. highly compressive data (right). (This figure is available in color online.)

= 0.2 (Hobbacher and Baumgartner 2024), but does not seem explicitly based on reliability and confidence considerations. At the same time, a $D << 1$ could cover LDA model assumptions (e.g. sequence effects are not taken into account), as well as a simplified resistance formulation (e.g. a linear or bi-linear one). In order to evaluate the GRFL formulation and GRNDA model performance, a comparison to recommended D values for design in guidelines and codes will be provided, aiming to quantify reliability and confidence.

A predicted lifetime N_{pred} incorporating a particular probability of survival p_s to ensure a sufficient level of reliability is basically a shift of the experimental one N_{exp} (e.g. Figures 9–12 right):

$$\log(N_{pred}) = \log(N_{exp}) \pm F^{-1}(p_s) \cdot \sigma_{VA}|_{c_l}. \qquad (23)$$

If the level of confidence c_l is not defined, the most likely

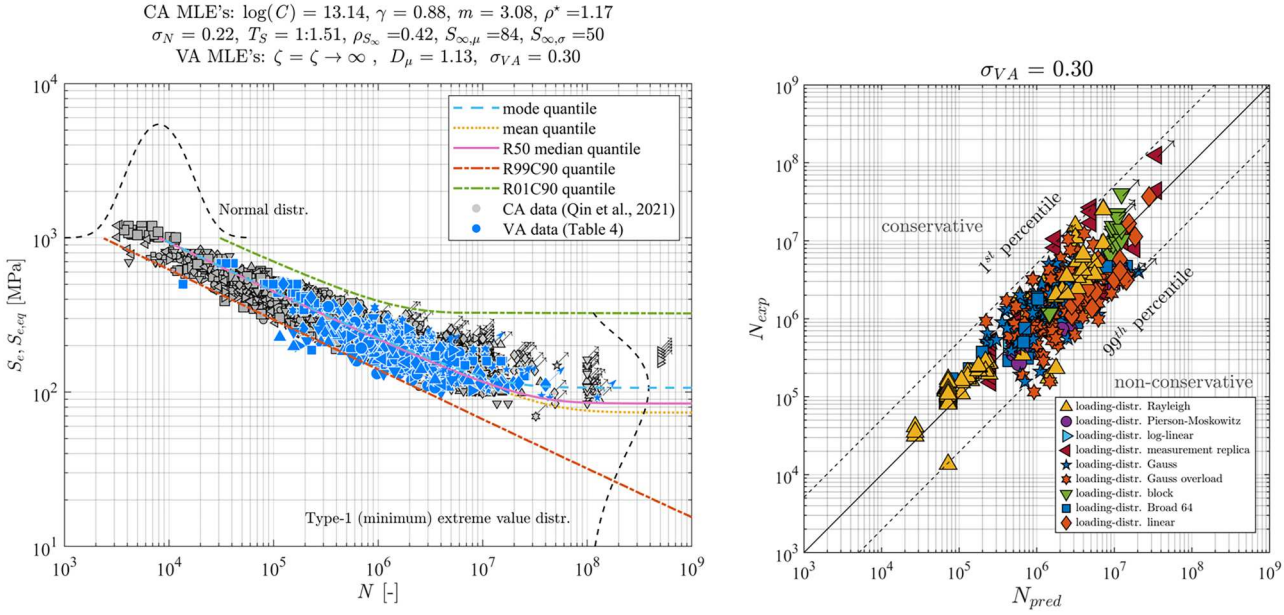

Figure 12. S_e-based VA MCF and HCF resistance formulation using a GRFL and GRNDA model with mean stress correction, but without VA HCF data (left), predicted vs experimental lifetime N for all the spectral distributions (right). (This figure is available in color online.)

Table 8. VA data scatter and damage estimates for the GRFL and GRNDA model, as well as IIW, DNV, and BS guideline and code evaluated with the RLDA model.

VA assessment	σ_{VA}	D_{μ}(R50)	D(R97)	D(R99C90)
S_e (average notch stress) – GRFL and GRND model	0.30	1.09	0.27	0.19
S_e (fictitious notch stress) – IIW-based	0.34	2.10	0.43	0.30
S_h (hot spot structural stress) – DNV-based	0.33	3.08	0.67	0.47
S_h (hot spot structural stress) – BS-based	0.33	3.11	0.67	0.48

σ_N is adopted. The inverse cumulative distribution function $F^{-1}(p_s)$ is typically of the Normal type (Section 2.2). Since the damage is lifetime dependent, naturally, the same distribution is involved (Section 3.1) to obtain a design estimate:

$$D(p_s) = 10^{\log(D_\mu) \pm F^{-1}(p_s)\cdot\sigma_{VA}|_{c_l}}. \quad (24)$$

For comparison, the IIW VA fatigue assessment procedure (Hobbacher and Baumgartner 2024), based on a fictitious notch stress S_e rather than an averaged notch stress one (Equation 1), as a fatigue strength parameter, is selected first. Following the guidelines (Fricke 2012), solid finite element models are used with a 1 mm notch radius and second-order element formulations. The CA resistance formulation is the FAT225-based bi-linear design curve: $\log(C_1) = 13.36$, $\log(C_2) = 17.60$, $m_1 = 3$, $m_2 = m_1 + 2 = 5$, with the slope change (Haibach 2006) at $N = 1{\cdot}10^7$ cycles. A random linear damage accumulation (RLDA) model is adopted, i.e., the LDA one with random damage $D(\mu, \sigma)$. Maximum Likelihood regression, similar to the GRFL and GRNDA models (Equation 14), using the bi-linear resistance curve formulation, provided the parameter vector $\theta_{VA} = \{D_\mu, \sigma_{VA}\}$ estimate (Table 8).

In comparison to the GRFL resistance and GRNDA model performance, the VA fatigue data scatter σ_{VA} has hardly increased (Table 8). The ζ exponent (Table 5 right, Figure 10, left) suggests damage accumulation behaviour close to linear, explaining the relatively good RLDA model performance.

Although the D_μ estimate is about twice as large (Table 8), a one-to-one comparison is inappropriate since for the fictitious S_e the bi-linear FAT225 design curve is involved, rather than the median as for the averaged S_e, and Maximum Likelihood regression aims to fit the VA data with respect to the involved resistance curve: $N_{pred} \rightarrow N_{exp}$ (Figure 13 left). For a damage level of reliability similar to a typical engineering resistance curve for design (R97), the damage estimate is between the IIW design values $0.2 < D < 0.5$. In case the same reliability and confidence levels are adopted (R99C90) as for the shown CA resistance quantile (Figure 10 left), the D estimate is still in the same range. For $D = 0.2$ as design criterion, quite some VA data sets show significant mean stress variations (Hobbacher and Baumgartner 2024); all predicted lifetime estimates are conservative (Figure 13 right).

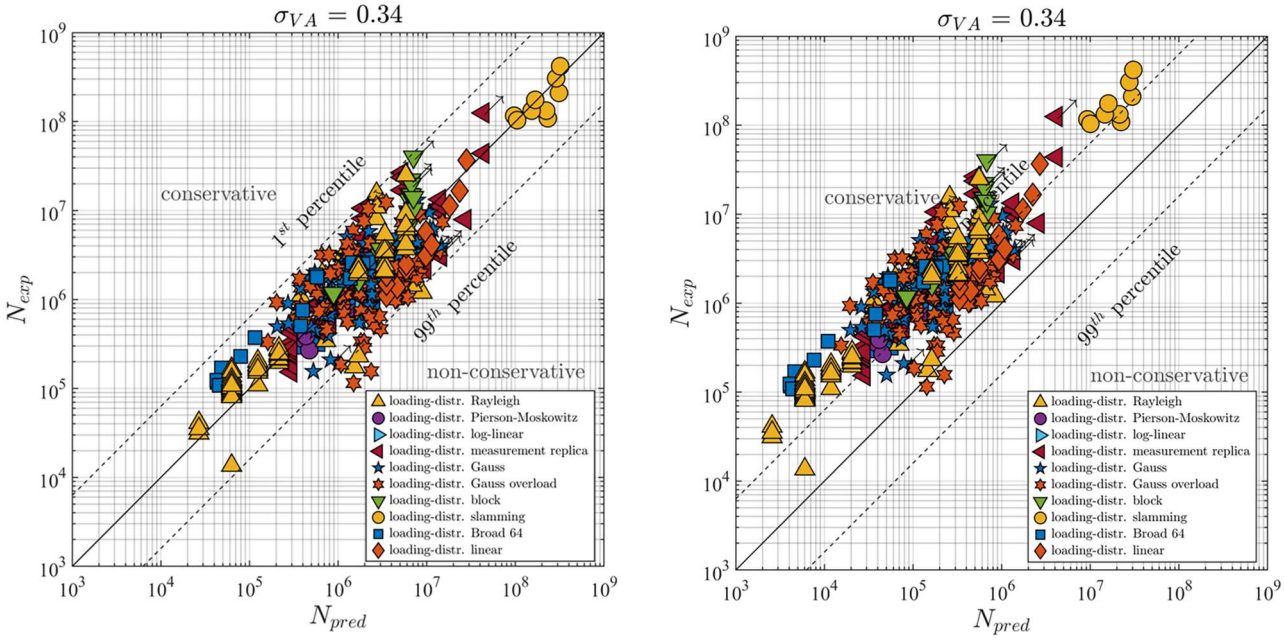

Figure 13. Predicted vs experimental lifetime N for an IIW VA fatigue assessment based on a fictitious notch stress S_e, a FAT225 bi-linear design curve and a RLDA model for D_μ (left) and $D = 0.2$ (right). (This figure is available in color online.)

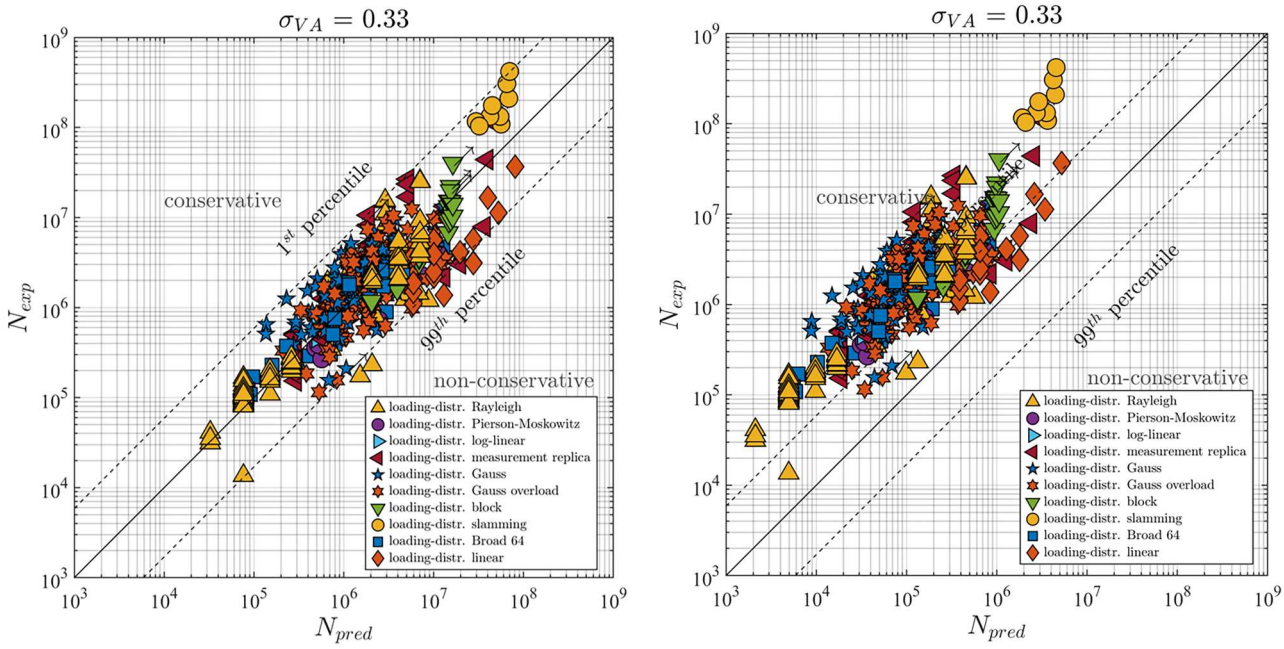

Figure 14. Predicted vs. experimental lifetime N for a DNV VA fatigue assessment based on a hot spot structural stress S_h, a bi-linear design curve 'D' (FAT90), and a RLDA accumulation model for D_μ (left) and $D = 0.2$ (right). (This figure is available in color online.)

Another comparison is based on the hot spot structural stress $S_h = \Delta\sigma_s$ as a fatigue strength parameter, obtained using through-thickness linearization rather than surface extrapolation (Dong and Hong 2003; Qin et al. 2019). The adopted CA resistance formulation is the bi-linear design curve 'D' (FAT90): $\log(C_1) = 12.16$, $\log(C_2) = 15.61$, $m_1 = 3$, $m_2 = m_1 + 2 = 5$, with the slope change at $N = 1{\cdot}10^7$ cycles (DNV 2024). Adopting the RLDA model, Maximum Likelihood regression provided the parameter vector $\theta_{VA} = \{D_\mu, \sigma_{VA}\}$ estimate (Table 8).

The VA fatigue scatter for S_h and S_e (both effective and fictitious) are similar, because of the approximately linear damage accumulation. However, D_μ obtained using S_h shows in comparison to the fictitious notch stress S_e a more conservative estimate for $N_{pred} = N_{exp}$

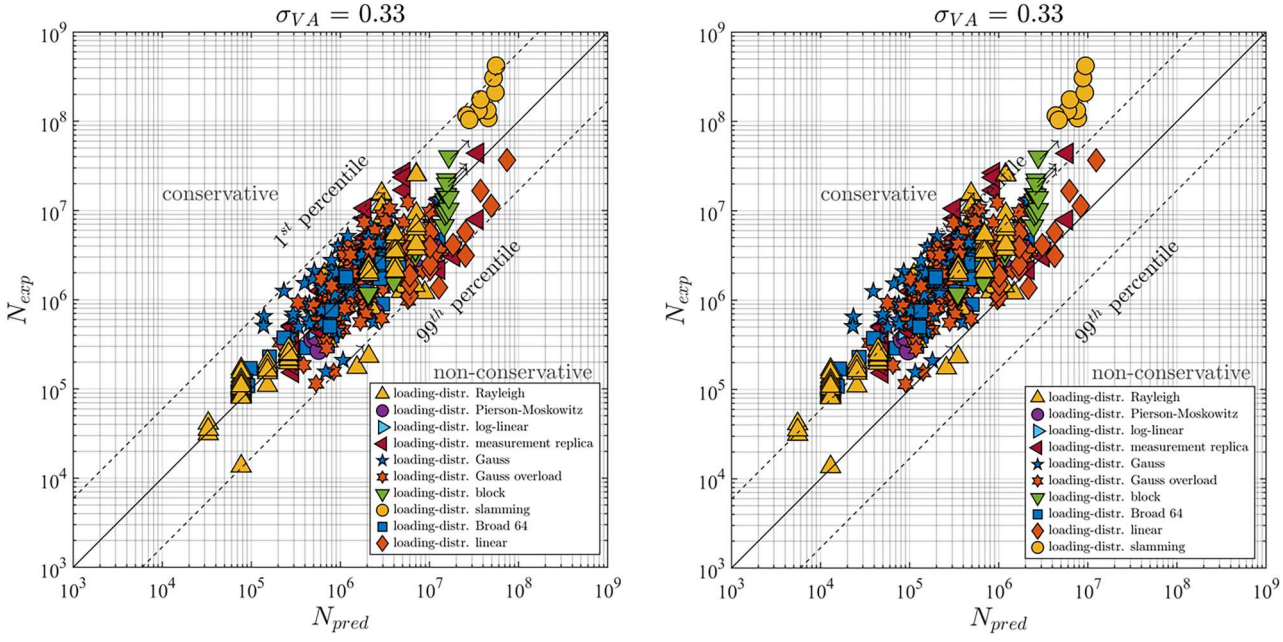

Figure 15. Predicted vs experimental lifetime N for a BS VA fatigue assessment based on a hot spot structural stress S_h, a bi-linear design curve 'D' and an RLDA accumulation model for D_μ (left) and $D = 0.5$ (right). (This figure is available in color online.)

(Figure 14,left, Table 8). The R97 and R99C90 damage estimates are in the $0.2 < D < 0.5$ range for design. Conservative lifetime estimates are obtained for $D = 0.2$ (Figure 14, right).

The BS (British Standard 2014) adopted a CA bi-linear design curve 'D' comparable to DNV with the parameters: $\log(C_1) = 12.18$, $\log(C_2) = 15.16$, $m_1 = 3$ and $m_2 = m_1 + 2 = 5$. However, the slope change is defined at $N = 5{\cdot}10^7$ cycles. Maximum Likelihood regression provided the parameter vector $\theta_{VA} = \{D_\mu, \sigma_{VA}\}$ estimate (Table 8). In comparison to DNV, D_μ is slightly larger because of the more conservative slope in the range of $N = 1{\cdot}10^7$ to $5{\cdot}10^7$ cycles, reflecting a smaller fatigue strength. At the same time, σ_{VA} hardly changed since the amount of VA HCF data is relatively small (Figure 15, left). The recommended damage value for high mean stress fluctuations, $D = 0.5$, is in good agreement with $D(\text{R99C90}) = 0.48$ and provides conservative lifetime estimates (Figure 15, right).

Finally, the damage design estimates for the CA GRFL resistance and VA GRNDA accumulation model, including global mean stress correction (Section 3.1) are obtained. Although differences are relatively small, σ_{VA} proves the best performance for the proposed model (Table 8). Note that D_μ is small in comparison to the IIW, DNV and BS-based estimates, since the median resistance curve is involved rather than a design-related one (Figure 11).

Ultimately, the design estimates for R97 and R99C90 are small as well, but as a result of all the reliability and confidence for VA assessment included in the damage, rather than both the CA-based resistance and the VA-related damage, like for the guidelines and codes (e.g. IIW, DNV, BS), avoiding double conservatism.

4. Conclusions and outlook

Adopting the averaged effective notch stress S_e as a fatigue strength parameter, a CA GRFL resistance formulation and a VA GRNDA model, CA-VA fatigue resistance similarity is achieved in the MCF and HCF regions, as reflected in $D_\mu \approx 1$. The scatter and performance parameter $\sigma_{VA} \approx 0.33$ suggests a similar lifetime scatter for CA and VA fatigue resistance data. In comparison to state-of-the-art guidelines and codes available for fatigue design, improved VA fatigue lifetime estimates are obtained using a frequency domain approach for arc-welded joints in steel (maritime) structures with different types of hot spots and a broad range of loading distributions.

The CA GRFL resistance formulation reveals a median quantile showing fatigue limit behaviour when shifting from MCF to HCF. Because of the fatigue limit $S_\infty(\mu, \sigma)$ uncertainties, a quantile for design (e.g. R99C90) shows approximately log–log linear behaviour, in contrast to a bi-linear one as typically used in guidelines and codes-based VA assessment. Fitting a statistically less performing bi-linear formulation to the CA data provides a similar observation for distinct MCF and HCF lifetime statistical distributions, a Normal and Extreme Value type-I maximum respectively, since the design quantile is a near log–log linear curve as well.

However, a typical VA (maritime) structural response reflects MCF and HCF resistance contributions, introducing a response history-dependent CA fatigue limit degradation; i.e., a response and resistance-induced damage accumulation non-linearity. The involved fatigue limit degradation exponent ζ proved to be particularly important for VA HCF, and the amount of data in this region is currently insufficient. In order to obtain an accurate ζ estimate with high confidence, VA tests with a focus on HCF data ($N \geq 10^8$) in terms of $S_{e,eq}$ are recommended. Since the obtained ζ reflects strong convex fatigue limit degradation, a LDA model turns out to be sufficient for VA data containing predominantly MCF content.

Incorporating a global mean stress effect – information typically available for a frequency domain approach – reduces the VA fatigue scatter and improves the CA-VA fatigue resistance similarity. Including mean stress on a cycle-by-cycle basis may provide another improvement. If strong sequence effects are expected (e.g. in case of specific block loading, overloading, or storm loading), a more computationally expensive time domain approach may be required. The mean stress correction currently employed is an exponential model with overall excellent performance, but appears to be not well-suited for fully compressive cycles yet. Since welding-induced (tensile) residual stresses are not explicitly incorporated, ignoring fully compressive cycles beforehand because of the required mode-I crack opening mode response conditions is inappropriate. At the same time, fully compressive response conditions are realistic for maritime applications and fatigue cracks can appear, like for a hogging/sagging-induced global mean stress component and a local water pressure-induced cyclic response around the water line. Both CA and VA HCF fatigue tests with fully compressive response conditions are recommended as input for both improved mean stress and VA damage accumulation modeling.

Finally, an important advantage of the proposed resistance formulation and damage model is that a particular probability of survival to ensure a sufficient level of reliability and even a confidence level can be defined

explicitly for VA fatigue assessment, based on the uncertainty in the VA data only. For structural design, $D = 0.2$ is recommended based on R99C90, i.e. $p_s = 0.99$ and $c_l = 0.90$, and involves the CA resistance median. The same damage value is provided in guidelines and codes (e.g. IIW, DNV) for VA conditions with highly fluctuating mean stress. Whereas the uncertainty for the proposed formulation and model is naturally accounted for in $D(\mu, \sigma)$ only, guidelines and codes use a resistance design curve reflecting a certain probability of survival and a maximum damage value without an assigned reliability and confidence level.

Author contributions

CRediT: **Ruben Leonard Geert Slange:** Conceptualization, Data curation, Formal analysis, Investigation, Methodology, Visualization, Writing – original draft, Writing – review & editing; **Marije Deul:** Conceptualization, Writing – review & editing; **Agnes Marie Horn:** Writing – review & editing; **Henk Den Besten:** Conceptualization, Funding acquisition, Methodology, Project administration, Supervision, Writing – review & editing.

Disclosure statement

No potential conflict of interest was reported by the author(s).

Funding

This publication is part of the project "FUSION: Smart Sensing for Informed Maintenance & Optimized Naval Design" (project number KICH1.VE-02.20.010) of the research programme "Maritime High-tech for Safer Seas", (partly) financed by the Dutch Research Council (NWO). The authors also gratefully acknowledge support from the FReady (Fleet Ready combination of physical and virtual hull structure monitoring) JIP.

Data availability statement

The analyzed fatigue test data are derived from resources available in the public domain: [Qin et al. 2021; Schilling et al. 1978; Albrecht and Friedland 1979; Albrecht et al. 1979; Fisher et al. 1983; Klippstein and Schilling 1989; Ota et al. 1997; Rörup and Petershagen 1999; Agerskov 2000; Demofonti et al. 2001; Zhang and Maddox 2009; Baptista et al. 2017; Yıldırım et al. 2020; Braun et al. 2022; Deul 2021; Duan et al. 2023; Leonetti et al. 2024].

ORCID

Ruben Leonard Geert Slange http://orcid.org/0009-0004-3030-9321
Marije Deul http://orcid.org/0009-0008-4141-9963
Henk Den Besten http://orcid.org/0000-0002-8726-218X

References

Agerskov H. 2000. Fatigue in steel structures under random loading. J Constr Steel Res. 53(3):283–305. https://doi.org/10.1016/S0143-974X(99)00042-5

Albrecht P, Friedland IM. 1979. Fatigue-limit effect on variable-amplitude fatigue of stiffeners. J Struct Div. 105(12):2657–2675. https://doi.org/10.1061/JSDEAG.0005316

Albrecht P, Yamada K. 1979. Simulation of service fatigue loads for short-span highway bridges. In: Service fatigue loads monitoring, simulation, and analysis255–277https://doi.org/10.1520/STP35877S.

Baptista C, Reis A, Nussbaumer A. 2017. Probabilistic S-N curves for constant and variable amplitude. Int J Fatigue. 101:312–327. https://doi.org/10.1016/j.ijfatigue.2017.01.022

Besten H. den. 2018. Fatigue damage criteria classification, modelling developments and trends for welded joints in marine structures. Ships Offsh Struct. 13(8):787–808. https://doi.org/10.1080/17445302.2018.1463609

Braun M, Dörner A, Willems T, Seidel M, Hendrikse H, Høyland K, Fischer C, Ehlers S et al. 2022. Fatigue strength of fixed offshore structures under variable amplitude loading due to wind, wave, and ice action. In: Proceedings of the ASME 2022 41st International Conference on Ocean, Offshore and Arctic Engineering. Volume 6: Polar and Arctic Sciences and Technology; June 5–10; Hamburg, Germany. V006T07A020. ASME; p. 1–7. https://doi.org/10.1115/OMAE2022-78764

British Standard. 2014. BS 7608:2014 guide to fatigue design and assessment of steel products. BSI.

Bufalari G, den Besten H, Kaminski ML. 2024. Mode-{I, III} multiaxial fatigue of welded joints in steel maritime structures: effective notch stress based resistance incorporating strength and mechanism contributions. Int J Fatigue. 180:108067. https://doi.org/10.1016/j.ijfatigue.2023.108067

CEN. 2025. EN 1993-1-9, Eurocode 3: design of steel structures – part 1-9: fatigue, March 2025. EUROPEAN COMMITTEE FOR STANDARDIZATION.

Ciavarella M, D'Antuono P, Demelio GP. 2017. A simple finding on variable amplitude (Gassner) fatigue SN curves obtained using Miner's rule for unnotched or notched specimen. Eng Fract Mech. 176:178–185. https://doi.org/10.1016/J.ENGFRACMECH.2017.03.005

Dekking FM, Kraaikamp C, Lopuhaä HP, Meester LE. 2005. A modern introduction to probability and statistics. Springer. https://doi.org/10.1007/1-84628-168-7

Demofonti G et al. 2001. High-strength steels in welded state for lightweight constructions under high and variable stress peaks.

Den Besten JH. 2015. Fatigue resistance of welded joints in aluminium high-speed craft: a total stress concept.

Deul ML. 2021. Fatigue damage accumulation in steel welded joints, subject to (random) variable amplitude loading conditions an improved fatigue-life model for naval ship structural design. http://repository.tudelft.nl/

DNV. 2024. DNV-RP-C203 recommended practice fatigue design of offshore steel structures. DNV.

Dong P, Hong JK. 2003. Analysis of Hot Spot Stress and Alternative Structural Stress Methods; 2003 22nd International Conference on Offshore Mechanics and

Arctic Engineering; Cancun, Mexico. https://doi.org/10.1115/OMAE2003-37315.
Duan H, Dang Z, Wei G. 2023. Damage distribution map based damage accumulation calculation approach for welded joints. Metals. 13(7):1203. https://doi.org/10.3390/met13071203
Fatemi A, Yangt L. 1998. Cumulative fatigue damage and life prediction theories: a survey of the state of the art for homogeneous materials. Int J Fatigue. 20(1):9–34. https://doi.org/10.1016/S0142-1123(97)00081-9
Fisher JW, Mertz DR, Zhong A. 1983. Steel bridge members under variable amplitude, long life fatigue loading. Transportation Research Board, National Research Council.
Fricke W. 2012. IIW recommendations for the fatigue assessment of welded structures by notch stress analysis: IIW-2006-09. Woodhead Publishing. https://doi.org/10.1533/9780857098566.
Fricke W, Paetzold H. 2014. Effect of whipping stresses on the fatigue damage of ship structures. Weld World. 58(2):261–268. https://doi.org/10.1007/s40194-014-0111-5
Gumbel EJ. 1954. Statistical theory of extreme values and some practical applications. A series of lectures. National Technical Reports Library - NTIS. https://ntrl.ntis.gov/NTRL/dashboard/searchResults/titleDetail/PB175818.xhtml
Gurney TR. 2006. Cumulative damage of welded joints. Woodhead Pub. and Maney Pub. on behalf of Institute of Materials, Minerals & Mining. http://www.amazon.com/exec/obidos/redirect?tag=citeulike07-20&path=ASIN/1855739380
Haibach E. 2006. Betriebsfestigkeit Verfahren und Daten zur Bauteilberechnung. Vol. 1. Berlin: Springer; p. 769. https://doi.org/10.1007/3-540-29364-7
Hectors K, De Waele W. 2021. Cumulative damage and life prediction models for high-cycle fatigue of metals: A review. Metals. 11(2):204–232. https://doi.org/10.3390/met11020204
Hobbacher AF, Baumgartner J. 2024. Recommendations for fatigue design of welded joints and components. Cham: Springer. https://doi.org/10.1007/978-3-031-57667-6
Johannesson P, Svensson T, De Maré J. 2005. Fatigue life prediction based on variable amplitude tests – methodology. Int J Fatigue. 27(8):954–965. https://doi.org/10.1016/j.ijfatigue.2004.11.009
Johnston C, Horn AM. 2024. Fatigue performance of riser quality girth welds: analysis of TWI and DNV's databases. Fatigue Fract Eng Mater Struct. 47:1482–1492. https://doi.org/10.1111/ffe.14248
Klippstein KH, Schilling CG. 1989. Pilot study on the constant and variable amplitude behavior of transverse stiffener welds. J Constr Steel Res. 12(3-4):229–252. https://doi.org/10.1016/0143-974X(89)90057-6
Kunz PM, Kulak GL. 1995. Fatigue safety of existing steel bridge. IABSE Rep. 73:1073–1078.
Leonetti D, Kinoshita K, Takai Y, Nussbaumer A. 2024. Fatigue behavior of transverse attachments under constant and variable amplitude loading from a Swiss motorway bridge. Int J Fatigue. 178:108003. https://doi.org/10.1016/j.ijfatigue.2023.108003
Leonetti D, Maljaars J, Snijder HH. 2020. Probabilistic fatigue resistance model for steel welded details under variable amplitude loading – inference and uncertainty estimation. Int J Fatigue. 135:105515. https://doi.org/10.1016/j.ijfatigue.2020.105515
Leonetti D, Maljaars J, Snijder HH (Bert). 2017. Fitting fatigue test data with a novel S-N curve using frequentist and Bayesian inference. Int J Fatigue. 105:128–143. https://doi.org/10.1016/J.IJFATIGUE.2017.08.024
Lotsberg I. 2025. Derivation of design S-N curves for butt welds in support structures for wind turbines. Marine Structures. 102:103795. https://doi.org/10.1016/j.marstruc.2025.103795
Mehmanparast A, Chahardehi A, Brennan F, Manzocchi M. 2024. Re-evaluation of fatigue design curves for offshore wind monopile foundations using thick as-welded test specimens. Eng Fail Anal. 158:107971. https://doi.org/10.1016/j.engfailanal.2024.107971
Miner MA. 1945. Cumulative damage in fatigue. J Appl Mech. 12(3):A159–A164. https://doi.org/10.1115/1.4009458
Naess A, Moan T. 2012. Stochastic dynamics of marine structures. Cambridge University Press.
Ota A, Maeda Y, Suzuki N. 1997. Fatigue strength of transverse butt welded joints under random loading. Application of Miner's rule in σ_{max}= $\sigma_y$tests. Weld Int. 11(12):958–965. https://doi.org/10.1080/09507119709447351
Qin Y, den Besten H, Palkar S, Kaminski ML. 2019. Fatigue design of welded double-sided T-joints and double-sided cruciform joints in steel marine structures: a total stress concept. Fatigue Fract Eng Mater Struct. 42(12):2674–2693. https://doi.org/10.1111/ffe.13089
Qin Y, den Besten H, Palkar S, Kaminski ML. 2021. Mid- and high-cycle fatigue of welded joints in steel marine structures: effective notch stress and total stress concept evaluations. Int J Fatigue. 142:105822. https://doi.org/10.1016/j.ijfatigue.2020.105822
Radaj D, Lazzarin P, Berto F. 2013. Generalised Neuber concept of fictitious notch rounding. Int J Fatigue. 51:105–115. https://doi.org/10.1016/J.IJFATIGUE.2013.01.005
Rörup J, Petershagen H. 1999. The effect of compression mean stresses on the fatigue strength.
Schijve J. 2009. Fatigue of structures and materials. Dordrecht: Springer; p. 1–622https://doi.org/10.1007/978-1-4020-6808-9.
Schilling CG, Klipstein KH, Barson JM, Blake GT. 1978. Fatigue of welded steel bridge members under variable amplitude loadings. Washington DC: Transportation research board, national research council.
Sonsino CM. 2007. Fatigue testing under variable amplitude loading. Int J Fatigue. 29(6):1080–1089. https://doi.org/10.1016/j.ijfatigue.2006.10.011
Sonsino CM. 2010. Effects on lifetime under spectrum loading*. Mater Test. 52(7-8):440–451.https://doi.org/10.3139/120.110146
Sonsino CM et al. 2012. Notch stress concepts for the fatigue assessment of welded joints – background and applications. Int J Fatigue. 34(1):2–16. https://doi.org/10.1016/J.IJFATIGUE.2010.04.011
Sonsino CM, Łagoda T, Demofonti G. 2004. Damage accumulation under variable amplitude loading of welded medium- and high-strength steels. Int J Fatigue. 26(5):487–495. https://doi.org/10.1016/j.ijfatigue.2003.10.001
Taylor D. 2008. The theory of critical distances. Engineering Fracture Mechanics. 75(7):1696–1705. https://doi.org/10.1016/j.engfracmech.2007.04.007

Walker K. 1970. Effects of environment and complex load history on fatigue life. ASTM Spec Tech Publ. STP 462:1–14. https://doi.org/10.1520/STP32032S

Yıldırım HC, Remes H, Nussbaumer A. 2020. Fatigue properties of as-welded and post-weld-treated high-strength steel joints: the influence of constant and variable amplitude loads. Int J Fatigue. 138:105687. https://doi.org/10.1016/j.ijfatigue.2020.105687

Zhang G, Sonsino CM, Sundermeier R. 2012. Method of effective stress for fatigue: part II – applications to V-notches and seam welds. Int J Fatigue. 37:24–40. https://doi.org/10.1016/J.IJFATIGUE.2011.09.016

Zhang YH, Maddox SJ. 2009. Investigation of fatigue damage to welded joints under variable amplitude loading spectra. Int J Fatigue. 31(1):138–152. https://doi.org/10.1016/j.ijfatigue.2008.04.006